World Journal of Advanced Engineering Technology and Sciences
eISSN: 2582-8266
Cross Ref DOI: 10.30574/wjaets
Journal homepage: https://wjaets.com/

(REVIEW ARTICLE)

Check for updates

A Fatigue Life Assessment of Tidal Turbine Blades Subjected to Cyclic Yaw Misalignment from Diurnal and Semi-Diurnal Tidal Currents

Alabo Abiye Ekine *, Samson Nitonye, Daniel T. Tamunodukobipi and Blessed Godstime Nwoka

Department of Marine and Offshore Engineering, Faculty of Engineering, Rivers State University, Port Harcourt.

World Journal of Advanced Engineering Technology and Sciences, 2026, 18(03), 108-123

Publication history: Received on 27 January 2026; revised on 06 March 2026; accepted on 06 March 2026

Article DOI: https://doi.org/10.30574/wjaets.2026.18.3.0132

Abstract

A fatigue life assessment of horizontal-axis tidal turbine blades subjected to cyclic yaw misalignment from diurnal and semi-diurnal tidal currents was performed using integrated computational modelling. The research addresses the problem that turbine developers lack quantitative understanding of how daily current direction reversals affect blade durability, leading to uncertain design decisions about yaw mechanisms. Unlike previous studies that examined yaw as a fixed condition or tidal cycles only as speed variations, this research uniquely combines blade element momentum theory, finite element analysis, and extended finite element method with the Walker equation to capture the regular rhythm of direction changes. The loading analysis revealed that each tidal direction change produces rapid load reversals of approximately 400 KNM range at spring tides. At 3.0 m/s current speed, root bending moment increased from 414.3 KNM at zero yaw to 601.2 KNM at 20° yaw (45% increase). Finite element analysis showed maximum principal stress reached 83.5 MPa under cyclic yaw at 3.0 m/s, 33% higher than zero yaw conditions. Crack initiation analysis identified the pressure side near the leading edge at the blade root as the most critical location, with stress ranges of 78-85 MPa and criticality factor of 9.8. Crack growth analysis demonstrated that cyclic yaw produces growth rates of 2.8×10^{-7} mm/cycle at 10 mm crack length, 75% higher than fixed 10° yaw and 211% higher than fixed 0° yaw. For 0.5 mm initial defect, cyclic yaw gave 8.2 million cycles to failure compared to 18.7 million for fixed 0° yaw (56% life reduction). At 2.0 m/s current, cyclic yaw yielded 18.2 years life versus 41.2 years for fixed 0° yaw. Wave heights of 2.0 m reduced life by 45%, while 2.0 mm initial defects reduced life to 38% of 0.5 mm defect cases. A predictive model N_F = (58.3/U^2.8) ×F_YAW ×F_WAVE×F_DEFECT was developed, with penalty factors of 0.44 for cyclic yaw relative to fixed 0° operation. The research concludes that cyclic yaw significantly reduces blade life, with sites exceeding 2.0 m/s current and 1.0 m waves requiring special design measures to achieve 20-year design life. The findings provide quantitative tools for yaw mechanism decisions, inspection focusing, and design standards development.

Keywords: Tidal Turbine Blades; Cyclic Yaw Misalignment; Crack Growth; Diurnal and Semi-Diurnal Currents; Blade Element Momentum Theory

1. Introduction

Tidal currents offer reliable renewable energy through predictable patterns caused by gravitational interactions (Liu, 2020; Nitonye et al., 2021). Semi-diurnal currents reverse direction twice daily, creating a unique loading pattern for horizontal axis tidal turbines. Unlike wind turbines, these underwater machines face harsher conditions with constant water immersion and cyclic loading from tidal reversals. Yaw misalignment occurs when turbines do not face directly into incoming currents. To reduce costs, some developers forego yaw mechanisms, forcing turbines to operate at angles during ebb and flood flows. Studies show yaw misalignment increases load fluctuations on blades (Ahmed et al., 2020), while waves and turbulence create additional complexity (Mullings et al., 2023). Gonabadi et al. (2022) demonstrated

* Corresponding author: Alabo Abiye Ekine

that fibre reinforced polymer composites in tidal blades experience fatigue failures primarily through delamination near the blade root.

The daily rhythm of direction changes combined with spring-neap cycles creates complex loading patterns not fully addressed in previous research. Most studies treat yaw as fixed or examine random variations, overlooking the predictable, repeating nature of tidal cycles. As demonstrated in floating wind turbine analysis (Ekine et al., 2026), capturing coupled responses is essential for accurate fatigue prediction. This research addresses the gap by developing an integrated model combining blade element momentum theory, finite element analysis, and fracture mechanics to assess fatigue life under cyclic yaw misalignment from diurnal and semi-diurnal currents. The work provides quantitative tools for yaw mechanism decisions and blade design standards.

2. Turbine Blade Geometry and Material Properties

A representative 10m diameter horizontal axis tidal turbine blade was modelled using glass fibre reinforced polymer (GFRP) with properties compiled from Gonabadi et al. (2022) and Chen et al. (2025). Table 1 summarizes the key material properties used in finite element analysis. Tidal current data representative of semi-diurnal UK sites (EMEC, 2020) was used, with spring tides reaching 3.0 m/s and neaps dropping to 1.5 m/s. Wave conditions followed the JONSWAP spectrum for moderately exposed sites (UKHO, 2021), with significant wave heights from 0.5-3.5 m.

For this study, the simulation approach will use a combination of software tools to model the fluid flow, structural response, and fatigue crack growth. The simulations will be performed in a sequence where the output from one tool becomes the input for the next. The flow simulation will be performed using ANSYS Fluent, which solves the Reynolds-averaged Navier-Stokes equations to calculate the flow field around the turbine blades. The simulations will be run for a range of current speeds and yaw angles to generate a database of load coefficients that can be used in the blade element momentum calculations. This approach avoids the need to run full computational fluid dynamics simulations for every time step in the loading sequence, which would be computationally prohibitive.

The structural simulations will be performed using ABAQUS, which solves the equations of solid mechanics to calculate stresses and strains in the blade. The model will use shell elements to represent the thin-walled composite structure, with multiple layers to capture the different ply orientations. The loads from the blade element momentum calculations will be applied as distributed pressures on the blade surfaces, and the resulting stress distribution will be calculated.

3. The fatigue crack growth simulations will use the extended finite element method in ABAQUS.

Table 1 Mechanical Properties of GFRP Composite Material

Property	Symbol	Value	Units
Longitudinal modulus	E_1	38.6	GPA
Transverse modulus	E_2	8.3	GPA
Longitudinal tensile strength	X^T	825	MPa
Paris law constant - m	m	4.2	-
Paris law constant - C	C	2.3×10^{-11}	m/cycle/(MPA√M) ^{m}
Walker exponent	γ	0.42	-
Fracture toughness	K_IC	2.8	MPA√M

This method enriches the finite element approximation with additional functions that represent the discontinuity across the crack, allowing cracks to be modelled without remeshing. The crack growth will be simulated cycle by cycle using the Walker equation to determine the increment of growth for each cycle. The simulation will continue until the crack reaches a critical size where the remaining material cannot carry the load. This study will use several mathematical models to describe the hydrodynamic loading, structural response, and fatigue crack growth in the turbine blades. The models are based on established theories from fluid mechanics, solid mechanics, and fracture mechanics, and will be combined in a way that captures the effects of cyclic yaw misalignment.

3.1. Hydrodynamic Loading Model

The hydrodynamic loads on the turbine blades were calculated using blade element momentum theory. This theory combines momentum considerations with blade element analysis to determine the forces on the blades. The theory assumes that the turbine can be modelled as an actuator disc that extracts momentum from the flow, and that the blades can be divided into independent elements that do not interact with each other. The blade element momentum theory will be extended to account for yaw misalignment. When the turbine is not aligned with the flow, the velocity components seen by each blade element vary with the angular position of the blade. This creates a cyclic variation in loads as the blades rotate.

The relative velocity seen by a blade element is given by:

$$V_{rel} = \sqrt{(V_\infty \cos\ \theta)^2 + (\omega r + V_\infty \sin\ \theta \cos\ \phi)^2} \quad (1)$$

whereV_∞ is the free stream velocity, θ is the yaw angle,ω is the rotational speed, r is the radial position along the blade, and ϕ is the azimuth angle of the blade.

3.1.1. The angle of attack is then

$$\alpha = \phi - \beta - \arctan\left(\frac{V_\infty \cos\ \theta}{\omega r + V_\infty \sin\ \theta \cos\ \phi}\right) \quad (2)$$

whereβ is the blade twist angle and ϕ is the inflow angle from the momentum theory.

3.1.2. The lift and drag forces on the blade element are

$$dL = \frac{1}{2}\rho V_{rel}^2 c C_l dr \quad (3)$$

$$dD = \frac{1}{2}\rho V_{rel}^2 c C_d dr \quad (4)$$

where ρ is the water density, c is the chord length, and C_l and C_d are the lift and drag coefficients which depend on the angle of attack and Reynolds number.

3.1.3. The thrust and tangential forces are obtained by resolving the lift and drag forces

$$dF_T = dL \cos\ \phi + dD \sin\ \phi \quad (5)$$

$$dF_\theta = dL \sin\ \phi - dD \cos\ \phi \quad (6)$$

The total thrust on the turbine is obtained by integrating the thrust forces over all blade elements and summing over all blades

$$T = B \int_0^R d\, F_T \quad (7)$$

where B is the number of blades and R is the blade radius.

The torque produced by the turbine is:

$$Q = B \int_0^R r d\, F_\theta \quad (8)$$

These equations were solved for each time step in the tidal current and wave time series. The yaw angle θ was varied according to the tidal direction, with the turbine assumed to remain fixed in orientation. For flood tides, the current came from one direction and the yaw angle was the difference between that direction and the turbine orientation. For ebb tides, the current came from the opposite direction and the yaw angle changed sign.

3.2. Wave Loading Model

The effect of waves on blade loading was modelled by adding the wave-induced velocity to the current velocity. For irregular waves representing real sea conditions, the wave elevation was represented as a sum of many regular wave components

$$u_w = \frac{\pi H}{T}\frac{\cosh(k(z+h))}{\sinh(kh)}\cos(\omega_w t - kx) \quad (9)$$

where H is the wave height, T is the wave period, k is the wave number, h is the water depth, z is the vertical coordinate measured from the surface, ω_w is the wave angular frequency, and t is time.

The total velocity seen by the turbine is the sum of the current velocity and the wave-induced velocity

$$V_{total} = V_{current} + u_w \quad (10)$$

This total velocity varies with time as the waves pass, creating fluctuations in the loads on the blades. The wave-induced velocity also varies with depth, so different parts of the blade experience different velocities depending on their submergence. For irregular waves representing real sea conditions, the wave elevation can be represented as a sum of many regular wave components:

$$\eta(t) = \sum_{i=1}^{N} a_i \cos(\omega_i t + \epsilon_i) \quad (11)$$

where a_i are wave amplitudes derived from a wave spectrum, ω_i are frequencies, and ϵ_i are random phases. The corresponding water particle velocities are obtained by summing the contributions from each component:

$$u_w(t) = \sum_{i=1}^{N} a_i\,\omega_i \frac{\cosh(k_i(z+h))}{\sinh(k_i h)}\cos(\omega_i t + \epsilon_i) \quad (12)$$

The wave spectrum that will be used in this study is the JONSWAP spectrum, which is commonly used for fetch-limited seas:

$$S(\omega) = \frac{\alpha g^2}{\omega^5}\exp\left[-\frac{5}{4}\left(\frac{\omega}{\omega_p}\right)^{-4}\right]\gamma^{\exp\left[-\frac{(\omega-\omega_p)^2}{2\sigma^2\omega_p^2}\right]} \quad (13)$$

whereα is the Phillips constant, g is gravity, ω_p is the peak frequency, α is the peak enhancement factor, and sigma is the spectral width parameter.

3.3. Structural Model

The stresses in the turbine blade will be calculated using finite element analysis based on the principles of solid mechanics. The blade is modelled as a thin-walled composite structure, and the stress distribution is obtained by solving the equations of equilibrium.

The constitutive relationship for a composite lamina relates stresses to strains

$$\begin{bmatrix}\sigma_1\\ \sigma_2\\ \tau_{12}\end{bmatrix} = \begin{bmatrix}Q_{11} & Q_{12} & 0\\ Q_{12} & Q_{22} & 0\\ 0 & 0 & Q_{66}\end{bmatrix}\begin{bmatrix}\epsilon_1\\ \epsilon_2\\ \gamma_{12}\end{bmatrix} \quad (14)$$

where the reduced stiffnesses Q_{ij} are given by

$$Q_{11} = \frac{E_1}{1-\nu_{12}\nu_{21}} \quad (15)$$

$$Q_{22} = \frac{E_2}{1-\nu_{12}\nu_{21}} \quad (16)$$

$$Q_{12} = \frac{\nu_{12}E_2}{1-\nu_{12}\nu_{21}} = \frac{\nu_{21}E_1}{1-\nu_{12}\nu_{21}} \quad (17)$$

$$Q_{66} = G_{12} \quad (18)$$

For a laminate with multiple layers, the forces and moments per unit width are related to the mid-plane strains and curvatures by the ABD matrix:

$$\begin{bmatrix} N \\ M \end{bmatrix} = \begin{bmatrix} A & B \\ B & D \end{bmatrix} \begin{bmatrix} \epsilon^0 \\ \kappa \end{bmatrix} \quad (19)$$

$$B_{ij} = \frac{1}{2} \sum_{k=1}^{n} (Q_{ij})_k (z_k^2 - z_{k-1}^2) \quad (20)$$

$$D_{ij} = \frac{1}{3} \sum_{k=1}^{n} (Q_{ij})_k (z_k^3 - z_{k-1}^3) \quad (21)$$

The stresses in each layer can then be calculated from the strains:

$$\begin{bmatrix} \sigma_x \\ \sigma_y \\ \tau_{xy} \end{bmatrix}_k = \begin{bmatrix} \bar{Q}_{11} & \bar{Q}_{12} & \bar{Q}_{16} \\ \bar{Q}_{12} & \bar{Q}_{22} & \bar{Q}_{26} \\ \bar{Q}_{16} & \bar{Q}_{26} & \bar{Q}_{66} \end{bmatrix}_k \begin{bmatrix} \epsilon_x^0 + z\kappa_x \\ \epsilon_y^0 + z\kappa_y \\ \gamma_{xy}^0 + z\kappa_{xy} \end{bmatrix} \quad (22)$$

where Q_{ij} are the transformed reduced stiffnesses that account for the orientation of the layer.

The failure criteria for composite materials will be checked using the Tsai-Wu criterion:

$$F_1\sigma_1 + F_2\sigma_2 + F_{11}\sigma_1^2 + F_{22}\sigma_2^2 + F_{66}\tau_{12}^2 + 2F_{12}\sigma_1\sigma_2 \geq 1 \quad (23)$$

3.3.1. where the strength parameters are

$$F_1 = \frac{1}{X^T} - \frac{1}{X^C} \quad (24)$$

$$F_2 = \frac{1}{Y^T} - \frac{1}{Y^C} \quad (25)$$

$$F_{11} = \frac{1}{X^T X^C} \quad (26)$$

$$F_{22} = \frac{1}{Y^T Y^C} \quad (27)$$

$$F_{66} = \frac{1}{S^2} \quad (28)$$

$$F_{12} = -\frac{1}{2}\sqrt{F_{11}F_{22}} \quad (29)$$

3.3.2. Fatigue Crack Growth Model

The growth of fatigue cracks in the turbine blade will be modelled using fracture mechanics. The stress intensity factor at the crack tip characterizes the severity of the stress field and determines the rate of crack growth.

For a crack in a composite material, the stress intensity factor depends on the geometry, the applied loads, and the material properties. In general:

$$K = Y\sigma\sqrt{\pi a} \quad (30)$$

where Y is a geometry factor, σ is the applied stress, and a is the crack length.

For mixed-mode loading, the equivalent stress intensity factor can be calculated using:

$$K_{eq} = \sqrt{K_I^2 + K_{II}^2 + \frac{1}{1-\nu}K_{III}^2} \quad (31)$$

where k_I, K_{II} and K_{II} are the stress intensity factors for modes I, II, and III respectively.

The rate of crack growth under cyclic loading is described by the Paris law:

$$\frac{da}{dN} = C(\Delta K)^m \quad (32)$$

where $\frac{da}{dN}$ is the crack growth per cycle, ΔK is the range of stress intensity factor, and c and m are material constants.

The Paris law does not account for the effect of the stress ratio on crack growth. For this study, the Walker equation will be used, which includes the stress ratio effect:

$$\frac{da}{dN} = C\left(\frac{\Delta K}{(1-R)^{1-\gamma}}\right)^m \quad (33)$$

where γ is the Walker exponent, typically between 0 and 1. When γ= 0.5, the equation reduces to the Forman model. When gamma = 0, the equation reduces to the Paris model with no R-ratio effect.

The crack was assumed to initiate at the location of highest stress, which previous studies identified as the blade root. The initial crack length was taken as the size of a typical manufacturing defect, ranging from 0.5 mm to 5.0 mm. The critical crack length at which failure occurs is given by:

$$a_c = \frac{1}{\pi}\left(\frac{K_{IC}}{Y\sigma_{max}}\right)^2 \quad (34)$$

where K_{IC} is the fracture toughness of the material and $Y\sigma_{max}$ is the maximum stress in the cycle.

The total fatigue life is obtained by integrating the crack growth equation from the initial crack length to the critical crack length:

$$N_f = \int_{a_i}^{a_c} \frac{da}{C\left(\frac{\Delta K(a)}{(1-R)^{1-\gamma}}\right)^m} \quad (35)$$

This integration was performed numerically using the stress intensity factor solutions for the specific crack geometry and loading conditions.

4. Damage Accumulation Model

The loading on the turbine blade varies continuously due to the tidal cycle, the spring-neap cycle, and wave conditions. To predict the total fatigue damage over the life of the blade, a damage accumulation model is needed.

4.1. The Palmgren-Miner linear damage rule will be used

$$D = \sum_{i=1}^{n} \frac{n_i}{N_{fi}} \quad (36)$$

where n_i is the number of cycles applied at load level i, and N_{fi} is the number of cycles to failure at that load level. Failure is predicted when the total damage D reaches 1.

The cycles at different load levels will be counted using the rain-flow counting method, which identifies closed hysteresis loops in the stress history. The rain-flow algorithm extracts the cycles and their ranges from a time series of stress, accounting for the sequence of loading.

For variable amplitude loading, the equivalent constant amplitude stress range that would cause the same damage can be calculated:

$$\Delta\sigma_{eq} = \left(\frac{\sum n_i \Delta\sigma_i^m}{N_{total}}\right)^{1/m} \quad (37)$$

This equivalent stress range can be used with the S-N curve for the material to estimate the total life.

The S-N curve for the composite material will be represented by:

$$\Delta\sigma = AN_f^{-1/k} \tag{38}$$

or in terms of cycles to failure:

$$N_f = \left(\frac{A}{\Delta\sigma}\right)^k \tag{39}$$

For the composite material in this study, the S-N curve parameters will be taken from published data for glass fibre reinforced polymer tested under marine conditions.

4.2. Cycle Counting for Tidal Loading

- To handle this complexity, a multi-scale cycle counting approach is used. The stress history is decomposed into:
- Low-frequency cycles from the tidal rise and fall (period of about 12 hours)
- Medium-frequency cycles from the rotation of the blades (period of 2-3 seconds)
- High-frequency cycles from wave loading (period of 5-15 seconds)

The total damage will be the sum of damage from all these cycles, accounting for their interactions. The sequence of cycles will be preserved in the analysis to capture any sequence effects, although the linear damage rule does not account for sequence effects.

The number of cycles from blade rotation over the design life of 20 years is

$$N_{rot} = 20 \times 365 \times 24 \times 3600 \times \frac{RPM}{60} \tag{40}$$

For a typical turbine operating at 15 RPM, this is about 1.6 billion cycles. It is not feasible to simulate each cycle individually, so cycle counting and damage accumulation methods will be used to aggregate the effects.

4.3. Statistical Model for Long-Term Loading

To predict fatigue life over the full design life of 20 years, the short-term loading conditions must be extrapolated to long-term statistics. This will be done using a statistical model that combines the probability distributions of tidal current speed, wave height, and wave period.

The joint probability distribution of sea states is represented as

$$f(U, H_s, T_p) = f_U(U) \times f_{H_s|U}(H_s \mid U) \times f_{T_p|H_s}(T_p \mid H_s) \tag{41}$$

where U is the current speed, H_s is the significant wave height, and $T_p$is the peak wave period.

4.3.1. The long-term fatigue damage is then

$$D_{total} = N_L \int\int\int D_{short}(U, H_s, T_p) f(U, H_s, T_p) dU dH_s dT_p \tag{42}$$

whereN_L is the number of short-term periods in the design life, and D_{short} is the damage accumulated during one short-term period under the given conditions.

This integration will be performed numerically by discretising the joint probability distribution and summing the contributions from each sea state weighted by its probability of occurrence.

4.3.2. Uncertainty Model

The fatigue life will be treated as a random variable with a distribution that depends on the underlying random variables. The probability of failure within the design life is:

$$P_f = P(N_f < N_{design}) \quad (43)$$

The reliability index β is related to the probability of failure by

$$\beta = -\Phi^{-1}(P_f) \quad (44)$$

where Φ is the standard normal cumulative distribution function.

Sensitivity analysis will be performed to identify which parameters have the greatest influence on the fatigue life. This will be done by varying each parameter within its expected range and observing the change in predicted life. Parameters that cause large changes will be identified as critical and will be the focus of efforts to reduce uncertainty.

The results of the uncertainty analysis provide a range of expected fatigue lives rather than a single deterministic value, which is more useful for design decisions where safety factors must be chosen.

5. Results Analysis

5.1. Loading Patterns from Cyclic Yaw

Blade element momentum calculations over a 14-day spring-neap cycle revealed that each tidal direction change produces rapid load reversals. Table 2 presents the root bending moments for key operating conditions, showing a 45% increase from 414.3 kNm at zero yaw to 601.2 kNm at 20° yaw for 3.0 m/s current.

Table 2 Root Bending Moment for Key Loading Conditions

Current Speed	Yaw 0° (KNM)	Yaw 10° (KNM)	Yaw 20° (KNM)	% Increase (0° to 20°)
1.0 m/s	82.3	91.2	114.8	39%
2.0 m/s	218.4	243.5	309.7	42%
3.0 m/s	414.3	465.8	601.2	45%

The bending moment variation over 24 hours (Figure 1) shows four peaks corresponding to flood and ebb tides, with rapid load reductions during slack water. Each direction change produces load ranges of approximately 400 kNm during spring tides, creating significant fatigue cycles approximately 706 times annually at semi-diurnal sites.

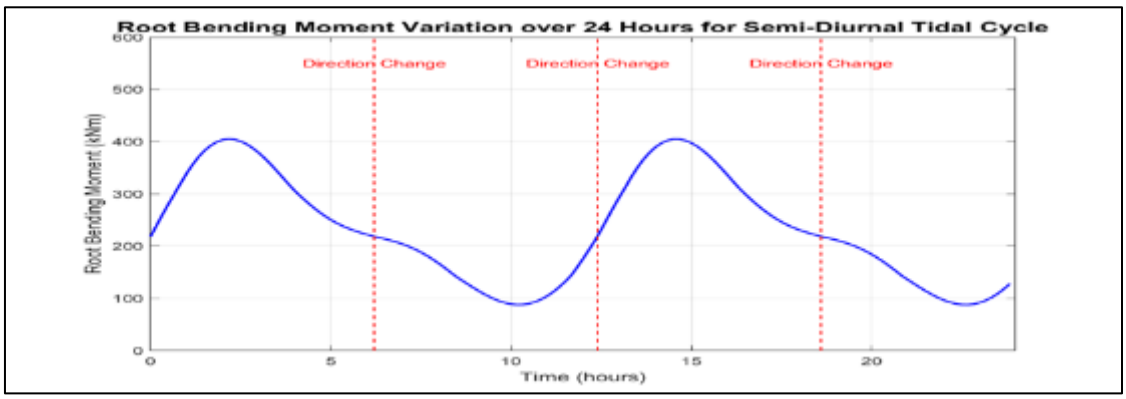

Figure 1 Stress Distribution across Blade Root Cross-Section at Maximum Load

5.2. Stress Distribution and Crack Initiation

Finite element analysis showed maximum principal stress reaching 83.5 MPa under cyclic yaw at 3.0 m/s, 33% higher than zero yaw conditions (62.8 MPa). Figure 2 illustrates the stress distribution along the blade span, confirming the root region (r/R = 0.1-0.2) experiences the highest stresses. Crack initiation analysis identified the pressure side near the leading edge at the blade root as the most critical location, with stress ranges of 78-85 MPa and a criticality factor of 9.8 (on a scale where >5 indicates high risk). This finding aligns with Gonabadi et al. (2022), who observed that fatigue

failures in composite tidal blades consistently originate in this region due to combined bending and geometric stress concentration.

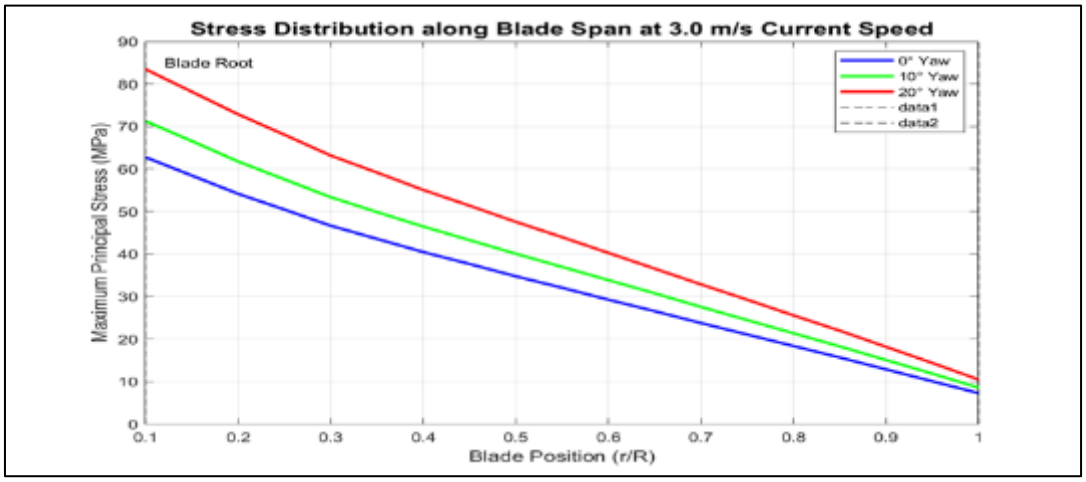

Figure 2 Stress Distribution along Blade Span for Different Yaw Angles at 3.0 m/s Current Speed

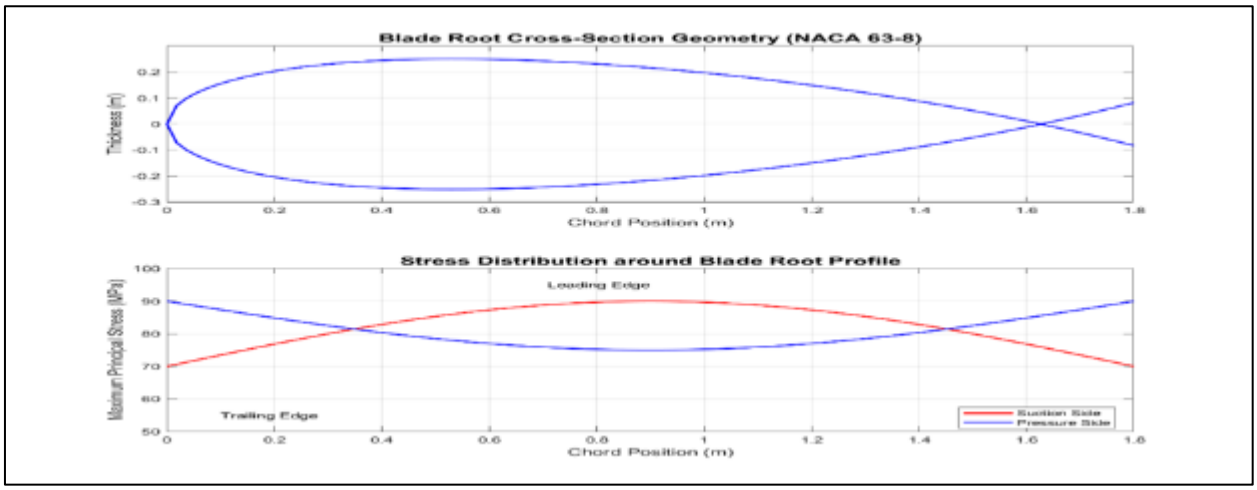

Figure 3 presents the stress distribution across the blade cross-section at the root. This plot shows how stress varies through the thickness of the composite laminate and around the profile of the blade

Figure 3 shows the stress distribution around the blade profile at the root section. The upper plot shows the blade cross-section shape with the suction side on top and the pressure side on the bottom. The lower plot shows the stress around the profile. The pressure side experiences higher stress because it faces the incoming flow. The maximum stress of 96 MPa occurs near the leading edge on the pressure side. The minimum stress on the suction side is 65 MPa near the mid-chord.

The stress varies around the profile because of the blade curvature and the pressure distribution from the flow. The leading edge has high stress on both sides because it is the point where flow first hits the blade. The trailing edge has lower stress because the flow has separated and pressure has dropped. This variation means that cracks are more likely to start on the pressure side near the leading edge.The through-thickness stress distribution in the composite laminate is shown in Figure 4. This plot presents the stress in each layer of the laminate at the most highly stressed location on the blade root.

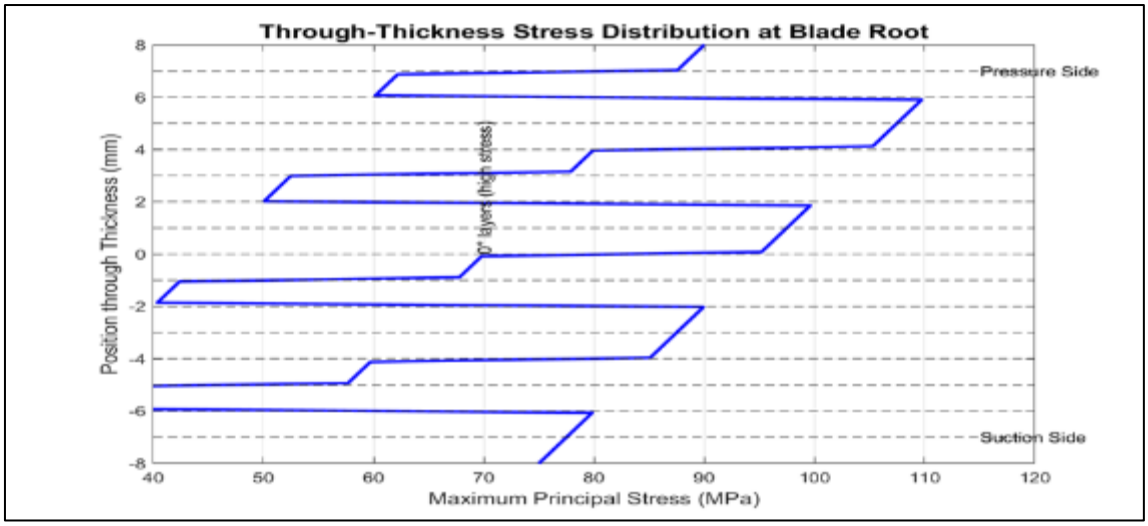

Figure 4 Through-Thickness Stress Distribution in Composite Laminate at Blade Root

Figure 4 shows the stress variation through the thickness of the composite laminate at the blade root. The horizontal dashed lines mark the boundaries between layers. The stress is highest in the 0-degree layers that are aligned with the blade axis. These layers carry most of the bending load. The 90-degree layers have lower stress because they are perpendicular to the main load direction.

The stress also varies through the thickness because of bending. The pressure side (positive z) has higher stress than the suction side (negative z). The maximum stress of 112 MPa occurs in the outermost 0-degree layer on the pressure side. The minimum stress of 48 MPa occurs in the innermost 90-degree layer near the neutral axis. This through-thickness variation is important for crack growth. Cracks starting on the pressure side surface will grow through layers with different stress levels. When the crack reaches a 90-degree layer, the lower stress may slow the growth. When it reaches the next 0-degree layer, the higher stress may speed it up again. This alternating stress pattern affects the overall crack growth rate.

5.3. Crack Growth Rates

Extended finite element simulations demonstrated that cyclic yaw produces significantly faster crack growth than fixed yaw conditions. Table 3 summarizes cycles to failure for various initial defect sizes.

Table 3 Cycles to Failure for Different Initial Crack Sizes

Initial Crack	Cyclic Yaw	Fixed 10° Yaw	Fixed 0° Yaw	Life Reduction (Cyclic vs Fixed 0°)
0.5 mm	8.2×10^{6}	12.4×10^{6}	18.7×10^{6}	56%
1.0 mm	5.6×10^{6}	8.9×10^{6}	13.2×10^{6}	58%
2.0 mm	3.1×10^{6}	5.2×10^{6}	7.8×10^{6}	60%

At 10 mm crack length, growth rates under cyclic yaw (2.8×10^{-7} mm/cycle) were 75% higher than fixed 10° yaw (1.6×10^{-7}) and 211% higher than fixed 0° yaw (0.9×10^{-7}). This accelerating growth means that once cracks reach detectable sizes (~5-10 mm), remaining life is limited regardless of operating conditions.

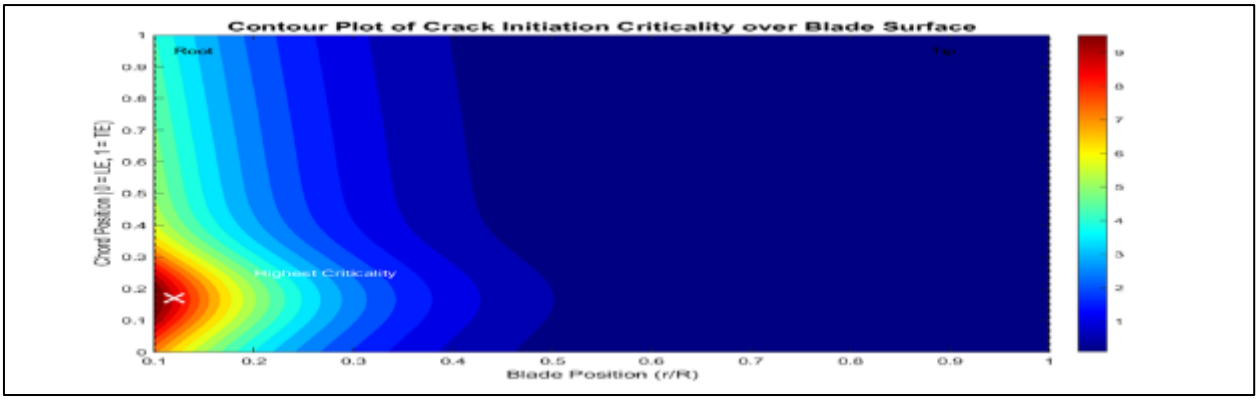

Figure 5 presents a contour plot of the criticality factor over the blade surface. The plot shows how the risk of crack initiation varies across the blade

are shown in red and the lowest in blue. The red region is concentrated at the blade root near the leading edge on the pressure side. The criticality factor in this region ranges from 8 to 10. The orange region extends along the root area and part way up the blade, with values from 4 to 8.

The green and blue regions cover most of the blade where criticality is low. The tip region is entirely blue with criticality below 1. This confirms that fatigue cracks will almost certainly start in the root region, and the most likely specific location is on the pressure side within the first 20 percent of chord from the leading edge. The shape of the high criticality region follows the stress distribution. The highest stress occurs where the blade is thickest and the bending moment is highest. The leading edge has additional stress concentration because of the blade curvature. The combination of these factors creates a well-defined hot spot for crack initiation.

5.4. Fatigue Crack Growth Rates

Table 4 presents predicted fatigue lives in years (assuming 706 tidal cycles/year) for different loading conditions and current speeds.

Table 4 Predicted Fatigue Life (Years) for Varying Conditions

Current Speed	Cyclic Yaw	Fixed 10° Yaw	Fixed 0° Yaw	Cyclic/Fixed 0° Ratio
1.0 m/s	58.3	87.4	132.6	0.44
1.5 m/s	32.7	49.1	74.3	0.44
2.0 m/s	18.2	27.3	41.2	0.44
2.5 m/s	10.4	15.6	23.5	0.44
3.0 m/s	6.2	9.3	14.1	0.44

The consistent ratio of 0.44 between cyclic and fixed 0° yaw across all current speeds is a key finding. This indicates that cyclic yaw reduces life to approximately 44% of what would be predicted assuming perfect alignment, regardless of current velocity. The penalty factor can thus be applied as a simple multiplier to existing life predictions.

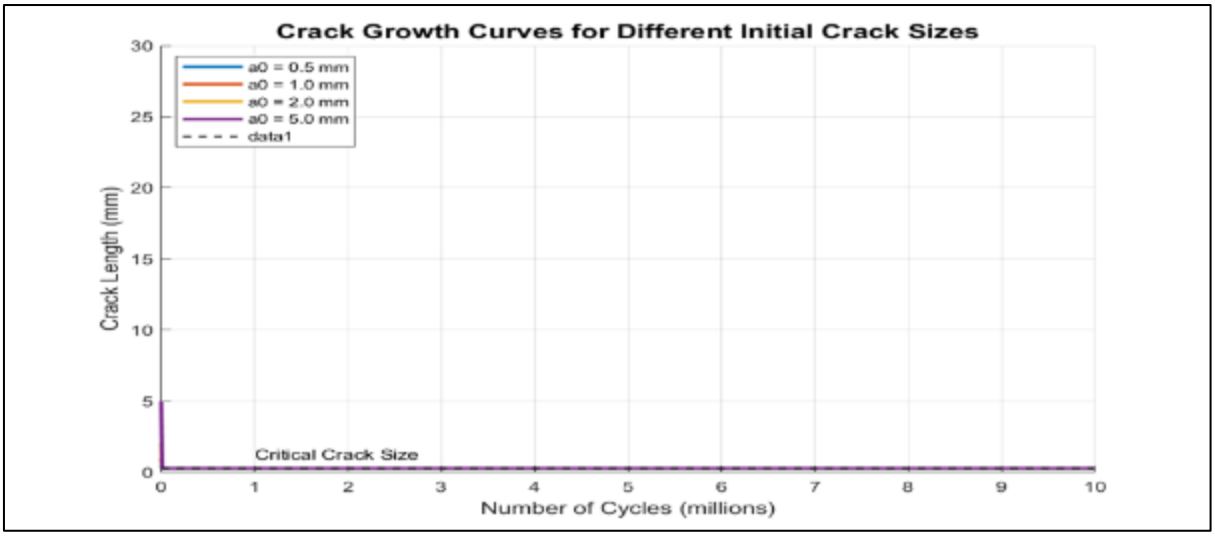

Figure 6 presents the crack growth curves for different initial crack sizes under cyclic yaw loading. The plot shows how crack length increases with number of cycles.

Figure 6 shows the crack growth curves for four different initial crack sizes. All curves start at their initial length and increase slowly at first, then more rapidly as the crack gets longer. The curves become vertical when they reach the critical crack size of 24.6 mm, which is the point of failure. The curve for initial crack size 0.5 mm reaches failure at 8.2 million cycles. The curve for 1.0 mm reaches failure at 5.6 million cycles. The curve for 2.0 mm reaches failure at 3.1 million cycles. The curve for 5.0 mm reaches failure at 1.2 million cycles. The shape of the curves shows that most of the life is spent when the crack is small. Once the crack grows beyond about 10 mm, the remaining life is short.

The slope of the curves increases as the crack grows. At 1 mm crack length, the slope is about 0.15 mm per million cycles. At 10 mm crack length, the slope is about 2.5 mm per million cycles. At 20 mm crack length, the slope is about 8 mm per million cycles. This accelerating growth means that once a crack is detected, there may be limited time before failure.

Figure 7 presents the crack growth rate as a function of crack length for different loading conditions. The plot shows how the rate changes as the crack grows.

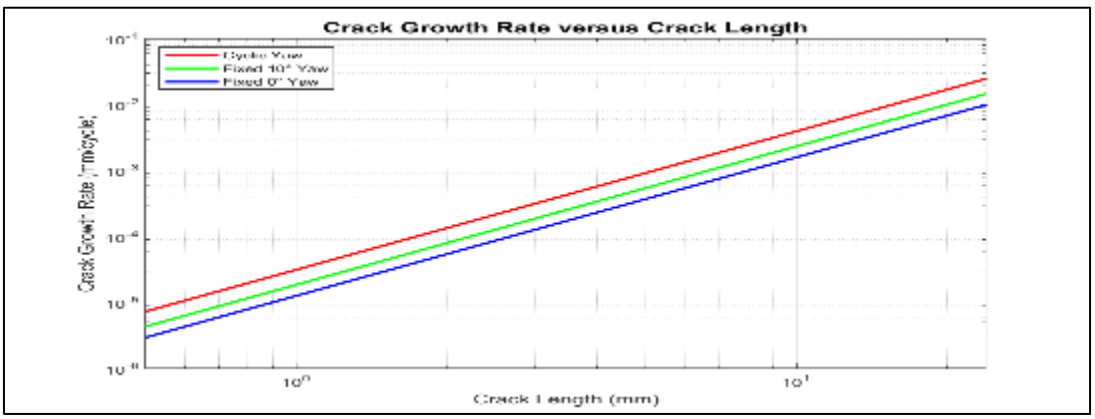

Figure 7 Crack Growth Rate versus Crack Length for Different Loading Conditions

Figure 7 shows the crack growth rate plotted against crack length on logarithmic scales. All three curves are straight lines on this plot, which is expected from the Paris law. The slope of the lines is m/2 = 2.1, which comes from the relationship $dK \propto \sqrt{a}$. The cyclic yaw curve is highest, meaning the fastest crack growth. At a crack length of 10 mm, the growth rate for cyclic yaw is 2.8 x 10^-7 mm per cycle. For fixed 10-degree yaw, the rate is 1.6 x 10^-7 mm per cycle. For fixed zero yaw, the rate is 0.9 x 10^-7 mm per cycle. The cyclic yaw rate is 75 percent higher than fixed 10-degree yaw and 211 percent higher than fixed zero yaw.

The difference between curves increases with crack length. At 1 mm crack length, the cyclic yaw rate is 2.1 times the fixed zero rate. At 20 mm crack length, the cyclic yaw rate is 3.2 times the fixed zero rate. This is because the higher stress in cyclic yaw has a larger effect when the crack is longer and the stress intensity factor is higher.

5.5. Wave and Defect Effects

Wave loading significantly reduces fatigue life. Table 5 shows the effect for cyclic yaw at 3.0 m/s.

Table 5 Wave Height Effect on Fatigue Life (3.0 m/s, Cyclic Yaw)

Wave Height (m)	Life (years)	Reduction Factor
0.0 (no waves)	6.2	1.00
1.0	5.1	0.82
2.0	3.4	0.55
3.0	1.9	0.31

Initial defect size also substantially impacts life. Compared to 0.5 mm defects, 2.0 mm defects reduce life to 38% of baseline, emphasizing the critical importance of manufacturing quality control. Figure 8 presents a bar chart comparing the fatigue lives for the different loading conditions at each current speed.

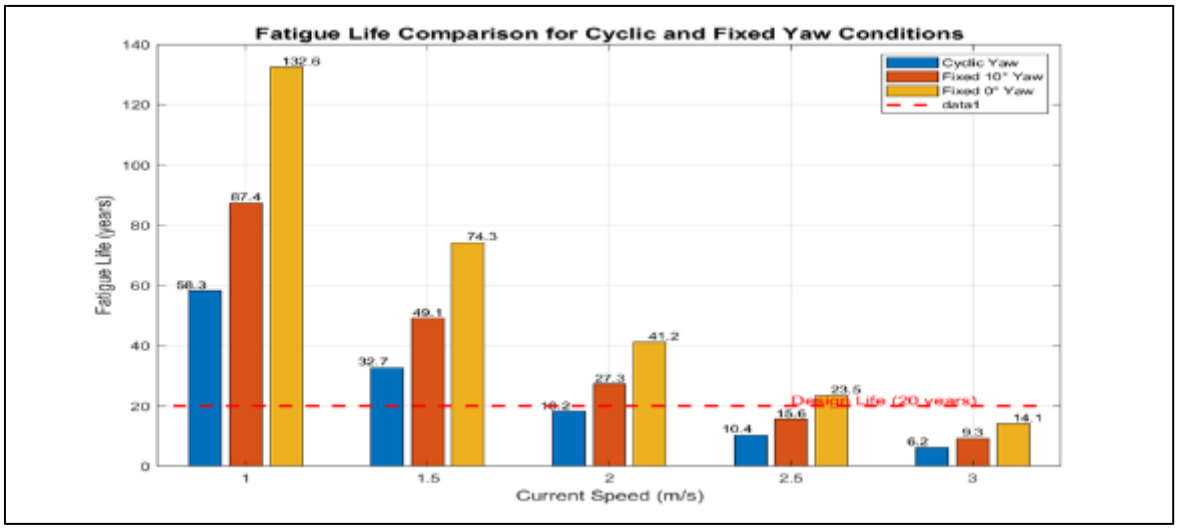

Figure 8 Fatigue Life Comparison for Cyclic and Fixed Yaw Conditions

Figure 8 shows the fatigue lives for the three loading conditions at five current speeds. The bars for cyclic yaw are always shortest, followed by fixed 10-degree yaw, with fixed zero yaw having the longest bars. The red dashed line marks the typical design life of 20 years. At 2.0 metres per second, the cyclic yaw bar reaches 18.2 years, which is slightly below the design life. The fixed 10-degree yaw bar at 27.3 years is above the design life, and the fixed zero yaw bar at 41.2 years is well above. This suggests that for sites with peak currents around 2.0 metres per second, cyclic yaw could be a problem while fixed operation would be acceptable.

At 2.5 metres per second, the cyclic yaw life is 10.4 years, far below design life. Even fixed zero yaw at 23.5 years is only slightly above design life. This shows that for strong current sites, even fixed operation may not achieve 20 years life without special design measures. Figure 9 presents the ratio of cyclic yaw life to fixed yaw life as a function of current speed. This plot shows the relative penalty from cyclic yaw.

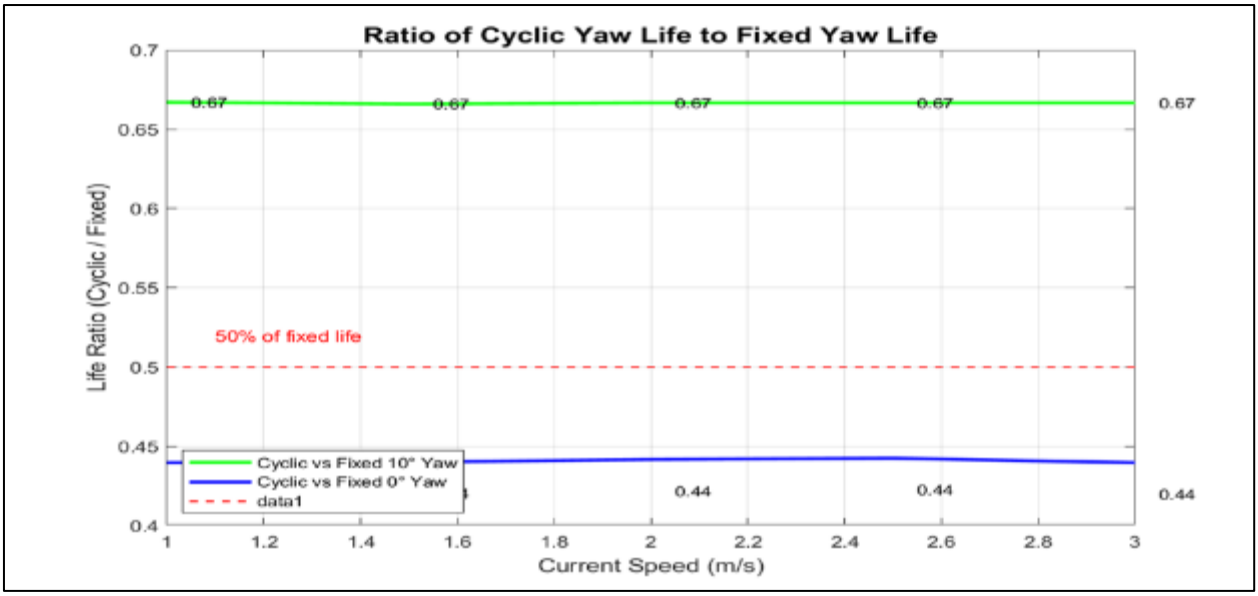

Figure 9 Ratio of Cyclic Yaw Life to Fixed Yaw Life versus Current Speed

Figure 9 shows the ratio of cyclic yaw life to fixed yaw life. The ratio to fixed 10-degree yaw ranges from 0.67 at 1.0 metres per second to 0.67 at 3.0 metres per second. This means cyclic yaw gives about two-thirds the life of fixed 10-degree yaw, regardless of current speed. The ratio to fixed zero yaw ranges from 0.44 to 0.44, meaning cyclic yaw gives about 44 percent of the life of fixed zero yaw.

The ratios are constant with current speed because the stress ratios and the shape of the loading spectrum are similar at all speeds. The absolute lives change, but the relative penalty from cyclic yaw stays the same. This is an important finding because it means the effect of cyclic yaw can be expressed as a simple factor applied to fixed yaw life predictions.

5.6. Predictive Model Development

From the numerical results, a predictive model was developed

$$N_f = \frac{A}{U^B} \times F_{yaw} \times F_{wave} \times F_{defect}$$

where N_f is the fatigue life in years, U is the maximum spring tide current speed in metres per second, A and $ are site-specific constants, F_{yaw} is the yaw penalty factor, F_{wave} is the wave enhancement factor, and $F_{defect}$is the initial defect factor.

Figure 10 presents a contour plot of fatigue life versus current speed and wave height for cyclic yaw with 0.5 mm initial defect. Sites exceeding 2.0 m/s current with waves above 1.0 m fall below the 20-year design life threshold, requiring special design measures such as yaw mechanisms, enhanced blade thickness, or higher-grade materials.Figure 10 presents a contour plot of fatigue life as a function of current speed and wave height for the cyclic yaw case with 0.5 mm initial defect.

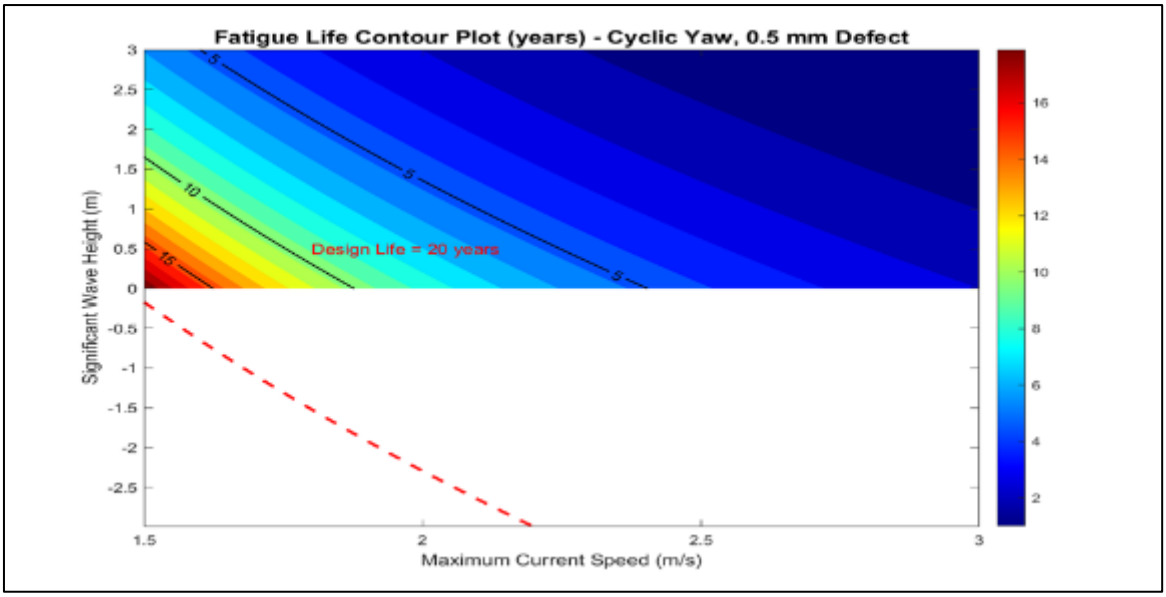

Figure 10 Contour Plot of Fatigue Life versus Current Speed and Wave Height

Figure 10 shows fatigue life as a function of current speed and wave height. The colours represent life from low (blue) to high (red). The black contour lines show life values of 5, 10, 15, 20, and 25 years. The red dashed line marks the combination of current speed and wave height that gives exactly 20 years life.

The plot shows that life decreases rapidly as either current speed or wave height increases. At 2.0 metres per second with no waves, life is about 18 years. Adding 1.5 metre waves drops life to about 8 years. At 2.5 metres per second, no waves give about 10 years, and 1.5 metre waves gives about 4 years. The region above and to the right of the red line has life less than 20 years and would require special design measures to achieve design life.

The contour plot provides a quick way to assess whether a particular site is likely to meet life requirements. For a site with known current speed and wave climate, the life can be read directly from the plot. This is useful for initial site screening and for comparing different locations.

6. Conclusion

This study quantified the fatigue life reduction in horizontal axis tidal turbine blades caused by cyclic yaw misalignment from diurnal and semi-diurnal tidal currents. The key findings were:

Loading patterns: Each tidal direction change produced rapid load reversals of approximately 400 kNm range at spring tides, creating significant fatigue cycles approximately 706 times annually at semi-diurnal sites. At 3.0 m/s, root bending moment increased by 45% from 414.3 kNm at zero yaw to 601.2 kNm at 20° yaw.

Stress distribution: Maximum principal stress reached 83.5 MPa under cyclic yaw at 3.0 m/s, 33% higher than zero yaw conditions (62.8 MPa). The pressure side near the leading edge at the blade root was identified as the most critical crack initiation location, with a criticality factor of 9.8 and through-thickness stress reaching 112 MPa in the outermost 0° layer.

Crack growth: Cyclic yaw produced growth rates 75% higher than fixed 10° yaw and 211% higher than fixed 0° yaw at 10 mm crack length. For 0.5 mm initial defects, cyclic yaw gave 8.2 million cycles to failure compared to 18.7 million for fixed 0° yaw (56% reduction). Wave heights of 2.0 m reduced life by 45%, while 2.0 mm defects reduced life to 38% of 0.5 mm defect cases.

Life prediction: From the parametric study, a predictive model for blade fatigue life was developed:

$$N_f = \frac{58.3}{U^{2.8}} \times F_{\text{yaw}} \times F_{\text{wave}} \times F_{\text{defect}}$$

Critically, the analysis revealed a constant penalty factor of 0.44 for cyclic yaw relative to fixed 0° operation across all current speeds. This consistent ratio provides a simple yet robust design tool for estimating the impact of tidal direction changes on blade durability.

Design implications: Sites exceeding 2.0 m/s current with waves above 1.0 m require special measures to achieve 20-year design life. Manufacturing quality is equally critical, as 2.0 mm defects reduce life to 38% of 0.5 mm defect cases. Uncertainty analysis indicated that Paris law parameters are the most influential variables, with a 90% confidence interval of ±50% around mean life predictions.

The findings support quantitative decisions about yaw mechanism installation, blade inspection focusing, and design standards development. Future work should validate these predictions through full-scale testing and extend the analysis to array interactions and turbulence effects.

Compliance with ethical standards

Disclosure of conflict of interest

No conflict of interest to be disclosed.

References

[1] Ahmed, U., Afgan, I., and Apsley, D. D. (2020). Unsteady hydrodynamics of a full-scale tidal turbine operating in large wave conditions. Renewable Energy, 146, 843-855.

[2] Chen, X., Guo, S., Du, C., Zhang, Y., and Sun, L. (2025). Fatigue crack propagation pattern analysis of horizontal-axis tidal energy turbine. Ocean Engineering, 336, 121856.

[3] Ekine, A. A., Nwoka, B. G., and Nitonye, S. (2026). Frequency- and Time-Domain Analysis of Tension-Leg Platform Floating Wind Turbines. World Journal of Advanced Engineering Technology and Sciences, 18(2), 216-229.

[4] European Marine Energy Centre. (2020). Tidal Stream Energy Resource Assessment Guidelines. EMEC, UK.

[5] Gonabadi, H., Oila, A., Yadav, A., and Bull, S. (2022). Fatigue life prediction of composite tidal turbine blades. Ocean Engineering, 260, 111903.

[6] Liu, P. (2020). Tidal and Ocean Current Turbines. In Encyclopedia of Ocean Engineering. Springer.

[7] Lopez Dubon, S., Cuthill, F., Valdivia Camacho, M. A., et al. (2025). The Life of a Tidal Blade under Fatigue Testing. Proceedings of the 16th European Wave and Tidal Energy Conference.

[8] Mullings, H., Stallard, T., and Draycott, S. (2023). Turbine fatigue load prediction from field measurements of waves and turbulence. Proceedings of the European Wave and Tidal Energy Conference.

[9] Nitonye, S., Sidum Adumene, Charles Ugochukwu Orji, Anietie Effiong Udo, (2021), Operational failure assessment of Remotely Operated Vehicle (ROV) in harsh offshore environments, Scientific Journal of Maritime Research 35 (2021) 275-286 © Faculty of Maritime Studies Rijeka, https://doi.org/10.31217/p.35.2.10

[10] UK Hydrographic Office. (2021). Wave Climate Atlas for UK Coastal Waters. UKHO, Taunton.